Charmonia production in pp collisions under NRQCD formalism

Vineet Kumar[1,2] and Prashant Shukla[1,2,*]

[1] *Nuclear Physics Division, Bhabha Atomic Research Center, Mumbai, India*

[2] *Homi Bhabha National Institute, Anushakti Nagar, Mumbai, India*

(Dated: February 26, 2016)

Abstract

In this work we calculate the high p_T quarkonia production cross section using NRQCD formalism. In NRQCD formalism quarkonia cross-section can be written as a product of short distance QCD cross-sections and long distance matrix elements (LDMEs). The short distance cross-sections can be calculated in terms of perturbative QCD and LDMEs are obtained using experimental data. We use measured data of ψ(2S), χ_c and J/ψ at 1.8, 1.96, 7 and 8 TeV to constrin LDMEs. These LDMEs are then used to calculate charmonia cross-section at 13 and 14 TeV.

PACS numbers: 12.38.Mh, 24.85.+p, 25.75.-q

Keywords: quark-gluon plasma, quarkonia, suppression, regeneration

* pshukla@barc.gov.in

I. INTRODUCTION

The study of quarkonia has yielded valuable insight into the nature of the strong interaction ever since the discovery of the J/ψ resonance [1, 2]. During the past three decades,$Q\bar{Q}$ bound states have provided useful laboratories for probing both perturbative and nonperturbative aspects of QCD. Quarkonia bound states are qualitatively different from most other hadrons since they are inherently nonrelativistic. The physics of quarkonia consequently involves several energy scales which are separated by the small velocity v of the heavy constituents inside $Q\bar{Q}$ bound states. In general one can subdivide the quarkonia production process into two major parts

1. Production of a heavy quark pair in hard collisions.

2. Formation of quarkonia out of the two heavy quarks.

Due to the high mass of the heavy quarks ($m_c \sim 1.5$ GeV/c^2, $m_b \sim 4.5$ GeV/c^2), they can be produced only during the first phase of a collision. Only at that time the elementary collisions with sufficiently high momentum transfers (to create such high masses) takes place. For this reason the heavy quark production is a hard process that can be treated perturbatively [3, 4], while the formation of quarkonia out of the two heavy quarks is a non purterbative process. The nonperturbative evolution of the $Q\bar{Q}$ pair into a quarkonium has been discussed extensively in terms of models and in terms of the language of effective theories of QCD [5, 6]. Different treatments of this evolution have led to various theoretical models for inclusive quarkonium production. Most notable among these are the color-singlet model (CSM), the color-evaporation model (CEM), the non-relativistic QCD (NRQCD) factorization approach, and the fragmentation-function approach.

The CSM was first proposed shortly after the discovery of the J/ψ [7–10]. In this model, it is assumed that the $Q\bar{Q}$ pair that evolves into the quarkonium is in a color-singlet state and that it has the same spin and angular-momentum quantum numbers as the quarkonium. In the CSM, the production rate for each quarkonium state is related to the absolute values of the color-singlet $Q\bar{Q}$ wave function and its derivatives, evaluated at zero $Q\bar{Q}$ separation. These quantities can be extracted by comparing theoretical expressions for quarkonium decay rates in the CSM with experimental measurements. Once this extraction has been carried out, the CSM has no free parameters. The CSM was successful in predicting quarko-

nium production rates at relatively low energy [11]. Recently, it has been found that, at high energies, very large corrections to the CSM appear at next-to-leading order (NLO) and next-to-next-to-leading order (NNLO) in α_s [12–14]. Consequently, the possibility that the CSM might embody an important production mechanism at high energies has re-emerged. However, given the very large corrections at NLO and NNLO, it is not clear that the perturbative expansion in α_s is convergent. As we will describe below, the NRQCD factorization approach encompasses the color-singlet model, but goes beyond it.

The CEM [15–17] is motivated by the principle of quark-hadron duality. In the CEM, it is assumed that every produced $Q\bar{Q}$ pair evolves into a quarkonium if it has an invariant mass that is less than the threshold for producing a pair of open-flavor heavy mesons. It is further assumed that the nonperturbative probability for the $Q\bar{Q}$ pair to evolve into a quarkonium state H is given by a constant F_H that is energy-momentum and process independent. Once F_H has been fixed by comparison with the measured total cross section for the production of the quarkonium H, the CEM can predict, with no additional free parameters, the momentum distribution of the quarkonium production rate. The CEM predictions provide good descriptions of the CDF data for J/ψ, ψ(2S), and χ_c production at $\sqrt{s} = 1.8$ TeV [17]. The CEM model has a full predicting power about cross-sections but it fails to predict the quarkonium polarization.

In the fragmentation-function approach the inclusive quarkonium production cross sections is written in terms of convolutions of parton production cross sections with light-cone fragmentation functions [18, 19]. This procedure provides a convenient way to organize the contributions to the cross section in terms of powers of m_Q/p. The contribution to the cross section at the leading power in m_Q/p_T is given by the production of a single parton (*e.g.*, a gluon), at a distance scale of order $1/p_T$, which subsequently fragments into a heavy quarkonium [20]. The contribution to the cross section at the first sub-leading power in m_Q/p_T is given by the production of a $Q\bar{Q}$ pair in a vector- or axial-vector state, at a distance scale of order $1/p_T$, which then fragments into a heavy quarkonium.

The NRQCD factorization approach [5] to heavy-quarkonium production is by far the most sound theoretically and most successful phenomenologically. The NRQCD factorization approach expresses the probability for a $Q\bar{Q}$ pair to evolve into a quarkonium in terms of matrix elements of NRQCD operators. These matrix elements can be characterized in terms of their scaling with the heavy-quark velocity v in the limit $v \ll 1$. A crucial feature

of this formalism is that it takes into account the complete structure of the $Q\bar{Q}$ Fock space, which is spanned by the state $n = {}^{2S+1}L_J^{[a]}$ with definite spin S, orbital angular momentum L, total angular momentum J, and color multiplicity a = 1, 8. In particular, this formalism predicts the existence of Color Octet (CO) processes in nature. This means that $Q\bar{Q}$ pairs are produced at short distances in CO states and subsequently evolve into physical, color-singlet (CS) quarkonia by the nonperturbative emission of soft gluons. In the limit $v \to 0$, the traditional CS model (CSM) is recovered in the case of S-wave quarkonia

In last few years, there is some very important progress in the NLO QCD correction calculation. The NLO corrections to color-singlet (CS) J/ψ hadroproduction have been investigated in Ref. [13, 21]. its transverse momentum distribution is found to be enhanced by 2-3 order of magnitude at high p_t region, and its polarization changes from transverse into longitudinal at NLO [21].The NLO corrections to J/ψ production via S-wave color octet (CO) states (${}^1S_0^{[8]}\,{}^3S_1^{[8]}$) are studied in Ref. [22] and the corrections to p_t distributions of both J/ψ yield and polarization are found to be small. In Refs. [23], NLO corrections for χ_{cJ} hadroproduction are studied.

The test of NRQCD factorization has been identified among the most critical milestones on the roadmap of quarkonium physics at the present time. While, for J/ψ polarization, comparisons of measured data with NRQCD predictions, unravel a rather confusing pattern [24–26], the situation is better for the J/ψ yield [26–28]. It has been shown that the set of CO LDMEs fitted to transverse-momentum (p_T) distributions measured at HERA and CDF lead to very good descriptions of the p_T distributions from RHIC and the LHC [27] On the other hand, the Tevatron data alone is not sufficient to constrain all the CO LDMEs [28] also the fit results of Ref. [27] and Ref [28] are incompatible with eachother.

After the continuous running of LHC for several years we now enter the era of precise quarkonia measurements. We now have very high quality quarkonia production data in several kinamatic regions up to very high transeverse momentum. In this paper we use this new data from LHC [29–31] along with the available data from CDF [32, 33] to constrain the LDMEs. These new LDMEs are then used to predict the J/ψ and ψ(2S) cross-section at 13 TeV for the kinematical bins relevant to LHC detectors.

II. QUARKONIA PRODUCTION IN P+P COLLISIONS

The factorization formalism of the NRQCD provides a theoretical framework for studying the heavy quarkonium production. The dominant processes in evaluating the differential yields of heavy mesons ψ as a function of p_T are the $2 \to 2$ processes of the kind $g+q \to \psi+q$, $q + \bar{q} \to \psi + g$ and $g + g \to \psi + g$, where ψ refers to the heavy meson. We label the process generically as $a + b \to \psi + X$, where a and b are the light incident partons. The invariant cross-section can be written in factorized form as

$$E\frac{d^3\sigma^{\psi}}{d^3p} = \sum_{a,b} \int\int dx_a\, dx_b G_{a/p}(x_a, \mu_F^2) G_{b/p}(x_b, \mu_F^2) \frac{\hat{s}}{\pi} \frac{d\sigma}{d\hat{t}} \otimes \delta(\hat{s} + \hat{t} + \hat{u} - M^2) \tag{1}$$

where, $G_{a/p}(G_{b/p})$ is the parton distribution function (PDF) of the incoming parton $a(b)$ in the incident proton, which depends on the momentum fraction $x_a(x_b)$ and the factorization scale μ_F as well as on the renormalization scale μ_R. However, as we have chosen $\mu_F = \mu_R$, in our case PDFs are function of x and μ_F only. The parton level cross-section $\mathrm{d}\sigma/\mathrm{d}\hat{t}$ is defined as []

$$\frac{d\sigma}{d\hat{t}} = \frac{d\sigma}{d\hat{t}}(ab \to Q\overline{Q}(^{2S+1}L_J) + X)\, M_L(Q\overline{Q}(^{2S+1}L_J) \to \psi) \tag{2}$$

The short distance contribution $d\sigma/d\hat{t}(ab \to Q\overline{Q}(^{2S+1}L_J) + X)$ can be calculated within the framework of perturbative QCD (pQCD). $M_L(Q\overline{Q}(^{2S+1}L_J) \to \psi)$ are the nonperturbative LDMEs and can only be estimated by comparison with experimental measurements. For $a + b \to \psi + X$ kind of processes the parton level Mandelstam variables $\hat{s}$, $\hat{t}$, and $\hat{u}$ can be expressed in terms of x_a, x_b as

$$\begin{aligned} \hat{s} &= x_a\, x_b\, s \\ \hat{t} &= M^2 - x_a \sqrt{s}\, m_T\, e^{-y} \\ \hat{u} &= M^2 - x_b \sqrt{s}\, m_T\, e^{y} \end{aligned} \tag{3}$$

where, $\sqrt{s}$ being the total energy in the centre-of-mass and y is the rapidity and p_T is the transverse momentum of the $Q\bar{Q}$. Writing down $\hat{s} + \hat{t} + \hat{u} - M^2 = 0$ and solving for x_b we obtain

$$x_b = \frac{1}{\sqrt{s}} \frac{x_a \sqrt{s}\, m_T\, e^{-y} - m_H^2}{x_a \sqrt{s} - m_T\, e^{y}}. \tag{4}$$

The double differential cross-section upon p_T and y takes the following form

$$\frac{d^2\sigma^{ab\to cd}}{dp_T\, dy} = \sum_{a,b} \int_{x_a^{min}}^{1} dx_a\, G_{a/A}(x_a,\, \mu_F^2)\, G_{b/B}(x_b,\, \mu_F^2) \times 2p_T \frac{x_a\, x_b}{x_a - \frac{m_T}{\sqrt{s}} e^{y}} \frac{d\sigma}{d\hat{t}}, \tag{5}$$

The minimum value of x_a is

$$x_{a\min} = \frac{1}{\sqrt{s}} \frac{\sqrt{s}\, m_T\, e^y - m_H^2}{\sqrt{s} - m_T\, e^{-y}}. \tag{6}$$

The short distance invariant differential cross-section is given by

$$\frac{d\sigma}{d\hat{t}}(ab \to Q\overline{Q}(^{2S+1}L_J) + X) = \frac{|\mathcal{M}|^2}{16\pi \hat{s}^2}, \tag{7}$$

$|\mathcal{M}|^2$ is the feynman squared amplitude averaged over initial spin of partons. In our calculations, we use the expressions for the short distance Color Singlet (CS) cross-sections given in Refs. [34–36] and the Color Octet (CO) cross-sections given in Refs. [37–39]. In our numerical computation, we use CTEQ6M [40] for the parton distribution functions. The LDMEs are predicted to scale with a definite power of the relative velocity v of the heavy constituents inside $Q\bar{Q}$ bound states. In the limit $v << 1$, the production of quarkonium is based on the $^3S_1^{[1]}$ and $^3P_J^{[1]}$ (J = 0,1,2) CS states and $^1S_0^{[8]}$, $^3S_1^{[8]}$ and $^3P_J^{[8]}$ CO states. The differential cross section for the direct production of J/ψ can be written as the sum of the contributions,

$$\begin{aligned} d\sigma(J/\psi) = {} & d\sigma(Q\bar{Q}([^3S_1]_1))\, M_L(Q\bar{Q}([^3S_1]_1) \to J/\psi) + d\sigma(Q\bar{Q}([^1S_0]_8))\, M_L(Q\bar{Q}([^1S_0]_8) \to J/\psi) \\ & + d\sigma(Q\bar{Q}([^3S_1]_8))\, M_L(Q\bar{Q}([^3S_1]_8) \to J/\psi) + d\sigma(Q\bar{Q}([^3P_0]_8))\, M_L(Q\bar{Q}([^3P_0]_8) \to J/\psi) \\ & + d\sigma(Q\bar{Q}([^3P_1]_8))\, M_L(Q\bar{Q}([^3P_1]_8) \to J/\psi) + d\sigma(Q\bar{Q}([^3P_2]_8))\, M_L(Q\bar{Q}([^3P_2]_8) \to J/\psi) \\ & + \cdots, \end{aligned} \tag{8}$$

where the quantity in the brackets [ ] represents the angular momentum quantum numbers of the $Q\bar{Q}$ pair in the Fock expansion. The subscript on [ ] refers to the color structure of the $Q\bar{Q}$ pair, 1 being the color-singlet and 8 being the color-octet. The dots represent terms which contribute at higher powers of v. The short distance cross sections $d\sigma(Q\bar{Q})$ correspond to the production of a $Q\bar{Q}$ pair in a particular color and spin configuration, while the long distance matrix element $M_L(Q\bar{Q}) \to J/\psi$ corresponds to the probability of the $Q\bar{Q}$ state to convert to the quarkonium wavefunction. This probability includes any necessary prompt emission of soft gluons to prepare a color neutral system that matches onto the corresponding Fock component of the quarkonium wavefunction. Power counting rules tell us that contributions from the color-octet matrix elements in Eq. 8 are suppressed by v^4 compared to the color singlet matrix elements.

The case of the p-wave bound states (χ_{c0}, χ_{c1}, and χ_{c2}, collectively referred to as χ_{cJ} is slightly different. The color-singlet state $Q\bar{Q}[^3P_J]_1$ and the color-octet state $Q\bar{Q}[^3S_1]_8$ contribute to the same order in v (v^5) because of the angular momentum barrier for $p-$wave states, and hence both need to be included for a consistent calculation in v. For the calculation of the production cross section, we consistently take the contributions to the lowest order in v. The χ_c differential cross section can be written as

$$d\sigma(\chi_{cJ}) = d\sigma(Q\bar{Q}([^3P_J]_1))\, M_L(Q\bar{Q}([^3P_J]_1) \to \chi_{cJ}) + d\sigma(Q\bar{Q}([^3S_1]_8))\, M_L(Q\bar{Q}([^3S_1]_8) \to \chi_{cJ}) + \cdots \tag{9}$$

Similar expressions hold for the $\chi_b(1P), \chi_b(2P)$ and $\chi_b(3P)$ mesons. Using above mentioned formalism we calculate the cross-section of charmonia states at LHC energies. For J/ψ production in $p-p$ collisions at LHC energies, three sources need to be considered: direct J/ψ production from initial parton-parton hard scattering, feed-down contributions to the J/ψ from the decay of heavier charmonium states, predominantly from $\psi(2S)$, χ_{c0}, χ_{c1} and χ_{c2} and J/ψ from B hadron decays. The sum of the first two sources is called "prompt J/ψ" and the third source is called "J/ψ from B". On the other hand, $\psi(2S)$ has no significant feed-down contributions from higher mass states. We call this direct contribution as "prompt $\psi(2S)$" to be consistent with the experiments. For the production of prompt J/ψ we consider the direct contribution, and feed-down contributions from $\chi_{c0}(1P)$, $\chi_{c1}(1P)$, $\chi_{c2}(1P)$ and $\psi(2S)$. The relevant branching fractions are given in Table I,

In this work, following [37, 38] we use the values of the color-singlet matrix elements calculated using the potential model. The expressions and the values for the color-singlet operators can be found in [37, 38, 41]. The values are obtained by solving the non-relativistic wavefunctions:

$$\begin{aligned}
&M_L(c\bar{c}([^3S_1]_1) \to J/\psi) = 3\, M_L(c\bar{c}([^1S_0]_1) \to J/\psi) = 3N_c \frac{|R_{n=1}(0)|^2}{2\pi} = 1.2 \text{ GeV}^3 \,, \\
&M_L(c\bar{c}([^3S_1]_1) \to \psi(2S)) = 3\, M_L(c\bar{c}([^1S_0]_1) \to \psi(2S)) = 3N_c \frac{|R_{n=2}(0)|^2}{2\pi} = 0.76 \text{ GeV}^3 \,, \\
&\frac{1}{5} M_L(c\bar{c}([^3P_2]_1) \to \chi_{c2}(1P)) = \frac{1}{3}\, M_L(c\bar{c}([^3P_1]_1) \to \chi_{c1}(1P)) = \, M_L(c\bar{c}([^3P_0]_1) \to \chi_{c0}(1P)) \\
&= 3N_c \frac{|R'_{n=1}(0)|^2}{2\pi} = 0.054\, m^2_{\text{charm}} \text{ GeV}^3.
\end{aligned} \tag{10}$$

Here $R(0)$ is the radial wavefunction at the origin, $R'(0)$ is the first derivative of the radial wavefunction at the origin, and n refers to the radial quantum number. We take the mass of the charm quark, $m_{charm} = 1.6$ GeV. The color-octet operators can not be related to the non-relativistic wavefunctions of $Q\bar{Q}$ since it involves a higher Fock state. We use measured data from LHC [29–31] and TeVatron [32] to constrain these Color Octet Matrix elements. For the net production of J/ψ we consider the direct contribution and feed-down contributions from $\chi_{c0}(1P)$, $\chi_{c1}(1P)$, $\chi_{c2}(1P)$ and $\psi(2S)$. Yields of $\psi(2S)$ have been measured at TeVatron [33] and LHC [29]. Data for χ_{cJ} is available from TeVatron [33].

TABLE I. Relevant branching fractions for charmonia [42]

Meson From	to χ_{c0}	to χ_{c1}	to χ_{c2}	to J/ψ
$\psi(2S)$	0.0962	0.092	0.0874	0.595
χ_{c0}				0.0116
χ_{c1}				0.344
χ_{c2}				0.195

The following color-singlet and color-octet contributions are relevant for our calculation.

1. Direct contributions

$$\begin{aligned} &M_L(c\bar{c}([^3S_1]_1) \to J/\psi) = 1.2\,\mathrm{GeV}^3 \\ &M_L(c\bar{c}([^3S_1]_8) \to J/\psi) \\ &M_L(c\bar{c}([^1S_0]_8) \to J/\psi) \\ &M_L(c\bar{c}([^3P_0]_8) \to J/\psi) \end{aligned} \tag{11}$$

2. Feed-down contribution from $\psi(2S)$

$$\begin{aligned} &M_L(c\bar{c}([^3S_1]_1) \to \psi(2S)) = 0.76\,\mathrm{GeV}^3 \\ &M_L(c\bar{c}([^3S_1]_8) \to \psi(2S)) \\ &M_L(c\bar{c}([^1S_0]_8) \to \psi(2S)) \\ &M_L(c\bar{c}([^3P_0]_8) \to \psi(2S)) \end{aligned} \tag{12}$$

3. Feed-down contribution from χ_{cJ}

$$M_L(c\bar{c}([^3P_0]_1) \to \chi_{c0}) = 0.054\, m_c^2\, \text{GeV}^3$$
$$M_L(c\bar{c}([^3S_1]_8) \to \chi_{c0}) \tag{13}$$

Hence for J/ψ we have to determine 10 parameters. Three color singlet matrix elements can be estimated from the wavefunctions of the heavy mesons. We use the following procedure to determine the remaining 7 color-octet components. CDF [33] has measured the feed-down contribution from the χ_{cJ} states to J/ψ production. We use this data to fit the color octet matrix element $M_L(Q\bar{Q}([^3S_1]_8) \to \chi_{c0})$. Figure 1 shows different components of cross-section along with the CDF data

$$M_L(Q\bar{Q}([^3S_1]_8) \to \chi_{c0})/m^2_{\text{charm}} = (0.00157 \pm 0.00159)\, \text{GeV}^3\ , \tag{14}$$

where the error includes the change in the matrix elements when we change the lowest p_T included in the fit by 1 GeV. The $\chi^2/dof = 4.56$ is not very good because the (dominant) color-octet production is harder than the experimentally observed spectrum. We assume that the measured yields of prompt $\psi(2S)$ is not substantially contaminated by higher feed-downs and use combined fit of the following data sets

1. CMS results at $\sqrt{S} = 7$ TeV [29, 30]
2. ATLAS results at $\sqrt{S} = 7$ and 8 TeV [31]
3. CDF results at $\sqrt{S} = 1.96$ TeV [32]

to obtain color octet $\psi(2S)$ matrix elements. Figure 2 and Figure 3 shows the fitted values of color-singlet and color-octet cross-section components along with the measured $\psi(2S)$ cross-section. We found following values of $\psi(2S)$ color-octet matrix elements

$$\begin{aligned} M_L(c\bar{c}([^3S_1]_8) \to \psi(2S)) &= (0.00190 \pm 0.00002)\, \text{GeV}^3 \\ M_L(c\bar{c}([^1S_0]_8) \to \psi(2S)) &= (0.0264 \pm 0.0003)\, \text{GeV}^3 \\ &= M_L(c\bar{c}([^3P_0]_8) \to \psi(2S))/m^2_{\text{charm}}\ , \end{aligned} \tag{15}$$

with a $\chi^2/dof = 00$. To fit the remaining 3 parameters we use the combined fit for the following results for J/ψ (direct+feed-down) yields

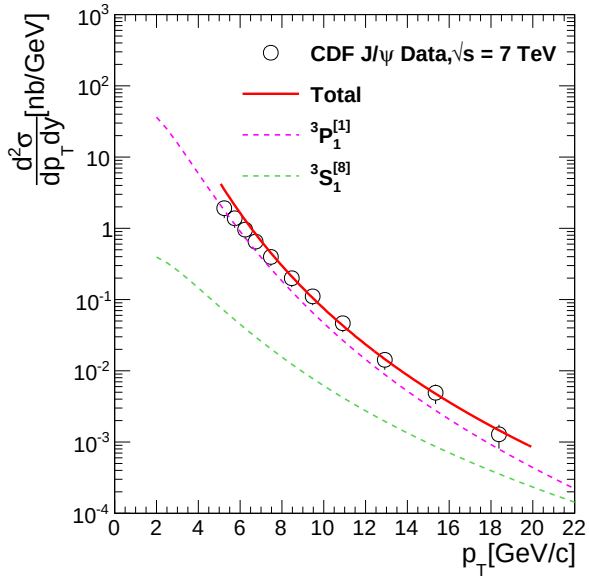

FIG. 1. (Color online) Differential production cross-section of J/ψ from χ_{c1} and χ_{c2} decays as a function of J/ψ p_T measured by CDF experiment at $\sqrt{s} = 1.8$ TeV [33]. We use these data sets to constrain color octet LDMEs. Figure also shows our calculations for various components of χ_c cross-section.

1. CMS results at $\sqrt{S} = 7$ TeV [29, 30]

2. ATLAS results at $\sqrt{S} = 7$ and 8 TeV [31]

3. CDF results at $\sqrt{S} = 1.96$ TeV [32]

Figure 4 and Figure 5 show the fitted values of color-singlet and color-octet cross-section components along with the measured J/ψ cross-section. Using simultaneous fitting of these data-sets we obtain,

$$\begin{aligned} M_L(c\bar{c}([^3S_1]_8) \to J/\psi) &= (0.00317 \pm 0.00007)\,\text{GeV}^3 \\ M_L(c\bar{c}([^1S_0]_8) \to J/\psi) &= (0.0630 \pm 0.0015)\,\text{GeV}^3 \\ &= M_L(c\bar{c}([^3P_0]_8) \to J/\psi)/m^2_{\text{charm}}\,, \end{aligned} \tag{16}$$

with a $\chi^2/dof = 0$. For a more sophisticated fitting of the color-octet matrix elements including NLO effects, see [24, 27].

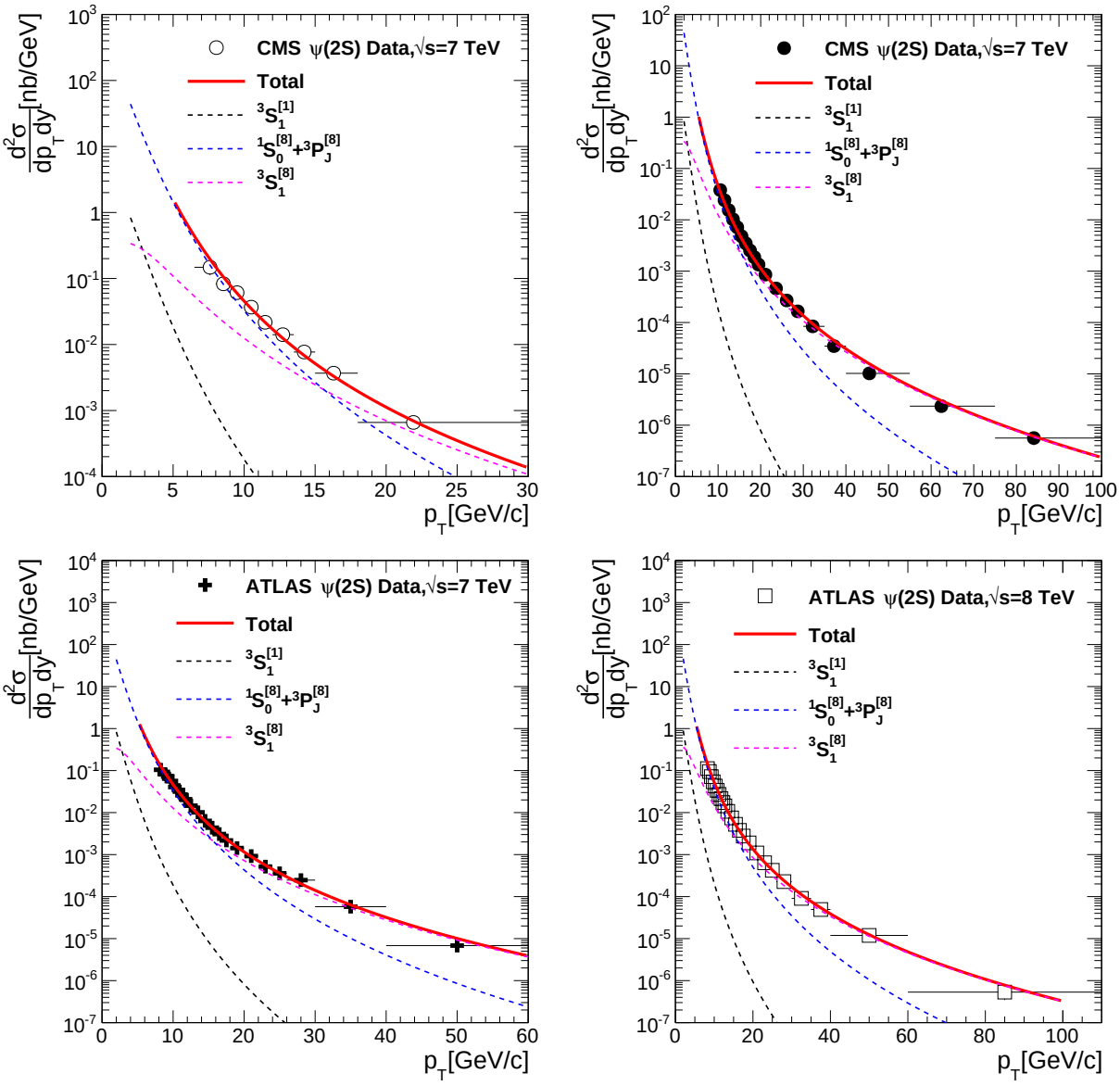

FIG. 2. (Color online) Differential production cross-section of $\psi(2S)$ as a function of p_T collected by LHC experiments at $\sqrt{s} = 7$ and 8 TeV [29–31]. We use these data sets to constrain color octet LDMEs. Figures also shows our calculations for various components of $\psi(2S)$ cross-section.

III. RESULT AND DISCUSSION

Figure 6 (a) shows the differential production cross-section of prompt J/ψ as a function of transeverse momentum (p_T) compared with the CMS measurements [30]. We have calculated differential production cross-sections for all the relevant resonances. These cross sections are then appropriately scaled with proper branching fractions and total cross section for prompt

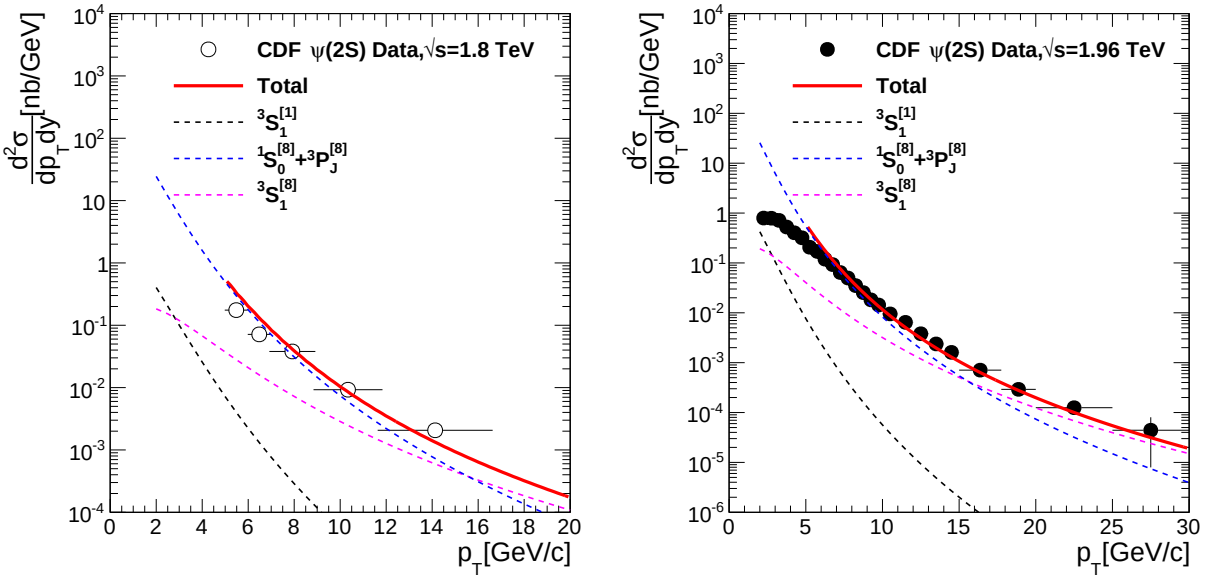

FIG. 3. (Color online) Differential production cross-section of ψ(2S) as a function of p_T collected by CDF experiment at $\sqrt{s} = 1.8$ TeV and $\sqrt{s} = 1.96$ TeV [32]. We use these data sets to constrain color octet LDMEs. Figures also shows our calculations for various components of ψ(2S) cross-section.

J/ψ is calculated and shown in Fig. 6 (a). The ψ(2S) has largest contribution at high p_T while at low p_T contribution from χ_{c1} and χ_{c2} exceed the ψ(2S) contribution. After adding all the contributions, the p_T dependence of prompt J/ψ differential production cross-section are described reasonably well by our calculations. The $\psi(2S)$ has no significant feed-down contributions from higher mass states. We call this direct contribution as "prompt ψ(2S)" to be consistent with the J/ψ calculations. Figure 6(b) shows the differential production cross-section of prompt ψ(2S) as a function of p_T compared with the CMS measurements [30]. Here also our calculations qualitatively reproduced the mesaured cross section.
Discription for old figures, should put new figures of cross section prediction at 14 TeV and describe the fitting figures.

IV. SUMMARY

We have calculated the differential production cross-section of prompt J/ψ and prompt ψ(2S) as a function of transverse momentum. For the J/ψ meson all the relevent contributions from higher mass states are estimated. The ψ(2S) meson does not have significant contributions from higher mass states. The calculations for prompt J/ψ and prompt ψ(2S)

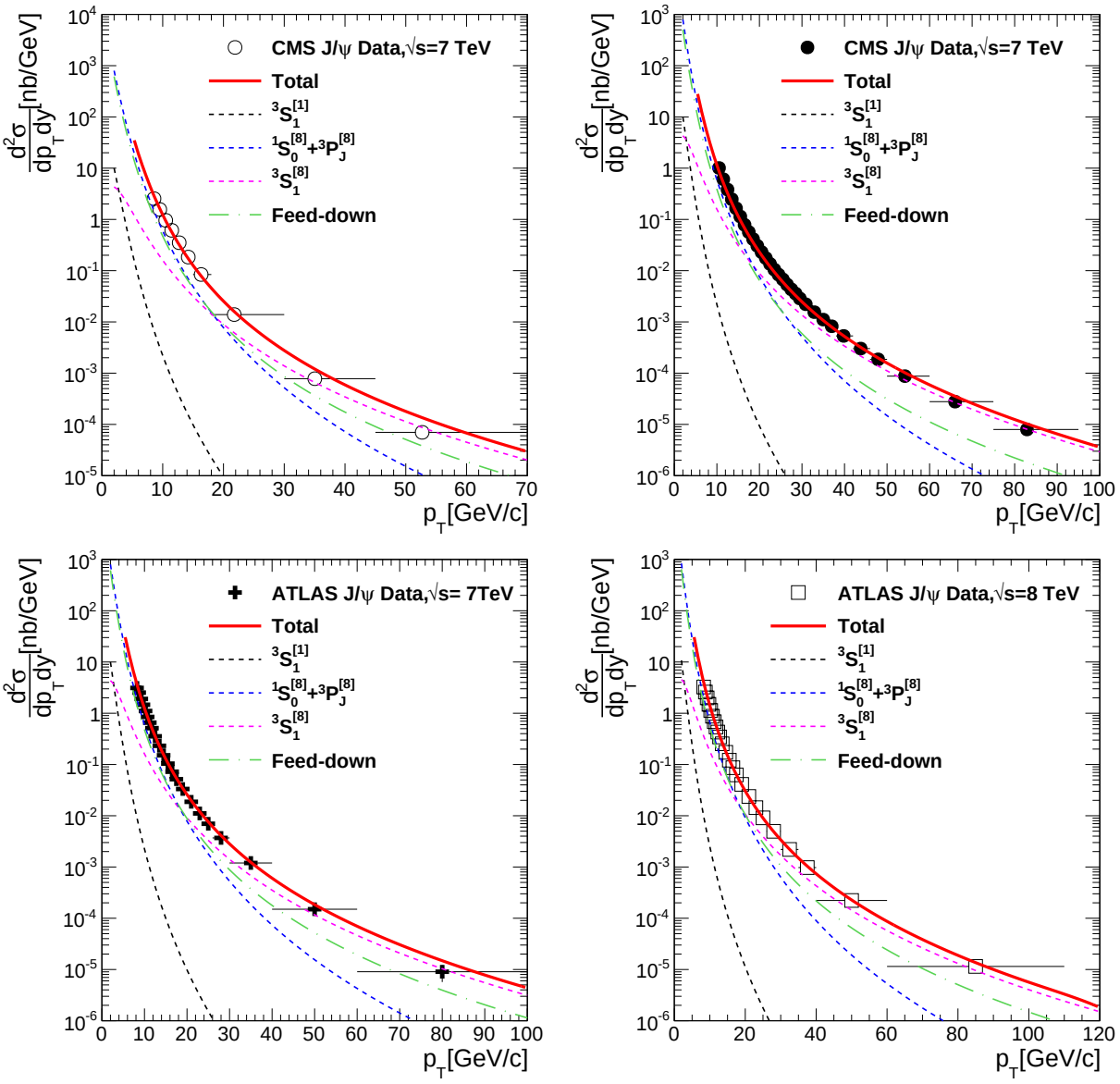

FIG. 4. (Color online) Differential production cross-section of J/ψ as a function of p_T collected by LHC experiments at $\sqrt{s} = 7$ and 8 TeV [29–31]. We use these data sets to constrain color octet LDMEs. Figures also shows our calculations for various components of J/ψ cross-section and feed-down contribution from higher charmonia states.

are compared with the measured data at LHC. A fairly good agreement between measured data and calculations is observed in low p_T range. The reevaluation of LDME is in progress using latest data from LHC to achieve good description of data in the whole p_T range.

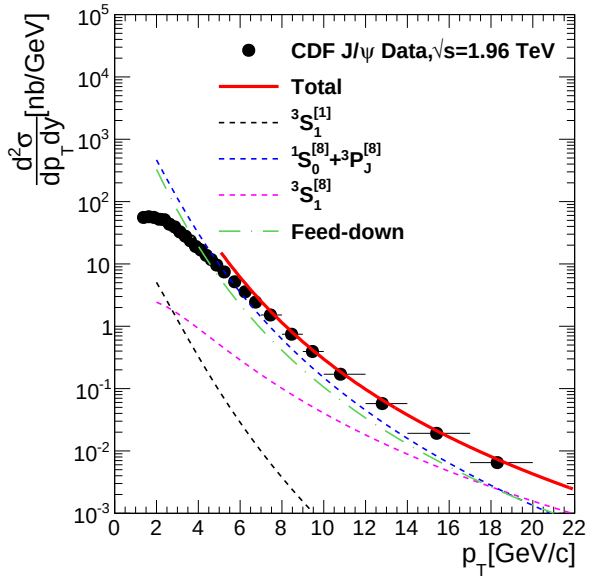

FIG. 5. (Color online) Differential production cross-section of J/ψ as a function of p_T collected by CDF experiment at $\sqrt{s} = 1.96$ TeV [32]. We use these data sets to constrain color octet LDMEs. Figures also shows our calculations for various components of J/ψ cross-section and feed-down contribution from higher charmonia states.

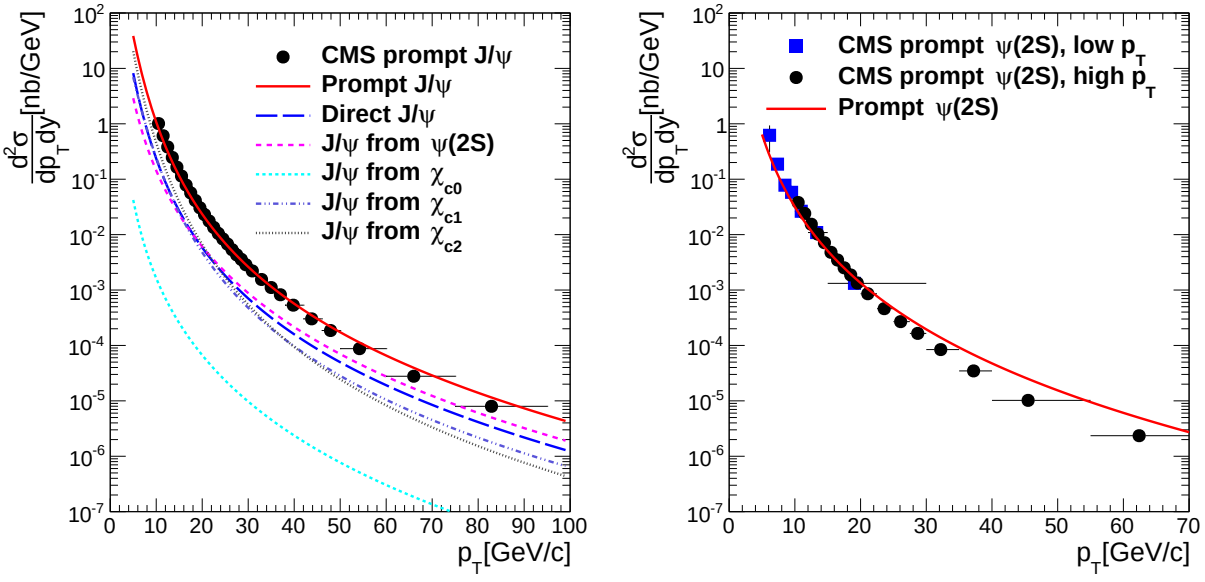

FIG. 6. (Color online) Differential production cross-section of J/ψ and ψ(2S) as a function of p_T compared with the CMS [29, 30] data.

Appendix A: Short distance pQCD cross sections for quarkonia production

Here we list the lowest order QCD cross sections for the resonance production used in our calculations. We write the formulas in terms of the invariants $\hat{s}$,$\hat{t}$,$\hat{u}$. where $\hat{s}^2+\hat{t}^2+\hat{u}^2=M^2$ and M is the mass of the resonance considered. The subprocesses of resonance production can be grouped as follows. To order α_s^2 one only has the gluon fusion processes, g g $\rightarrow^{(2S+1)}$ L_J. This process gives resonance with very small p_T, so we do not use these cross-sections in our calculations.

To order α_s^3, on the other hand, one has typically two-by-two scattering processes. The relevant cross sections are given below:

a. Color Singlet PQCD cross sections

- g q $\rightarrow$ $^{(2S+1)}$L$_J$ q or (q$\rightarrow$ $\bar{q}$)

$$\begin{aligned}
\frac{d\sigma}{d\hat{t}}(^1S_0) =& \frac{2\pi {\alpha_s}^3 (R_0)^2}{9M\hat{s}^2}\cdot\frac{(\hat{t}-M^2)^2-2\hat{s}\hat{u}}{(-\hat{t})(\hat{t}-M^2)^2}\\
\frac{d\sigma}{d\hat{t}}(^3P_0) =& \frac{8\pi {\alpha_s}^3 (R'_1)^2}{9M^3\hat{s}^2}\cdot\frac{(\hat{t}-3M^2)^2(\hat{s}^2+\hat{u}^2)}{(-\hat{t})(\hat{t}-M^2)^4}\\
\frac{d\sigma}{d\hat{t}}(^3P_1) =& \frac{16\pi {\alpha_s}^3 (R'_1)^2}{3M^3\hat{s}^2}\cdot\frac{-\hat{t}(\hat{s}^2+\hat{u}^2)-4M^2\hat{s}\hat{u}}{(\hat{t}-M^2)^4}\\
\frac{d\sigma}{d\hat{t}}(^3P_2) =& \frac{16\pi {\alpha_s}^3 (R'_1)^2}{9M^3\hat{s}^2}\cdot\\
& \frac{(\hat{t}-M^2)^2(\hat{t}^2+6M^4)-2\hat{s}\hat{u}(\hat{t}^2-6M^2(\hat{t}-M^2))}{(-\hat{t})(\hat{t}-M^2)^4}
\end{aligned} \tag{A1}$$

- q $\bar{q}$ $\rightarrow$ $^{(2S+1)}$L$_J$ g

$$\frac{d\sigma}{d\hat{t}}(^{(2S+1)}L_J) = -\frac{8}{3}\frac{\hat{t}^2}{\hat{s}^2}\frac{d\sigma}{d\hat{t}}(gq\rightarrow^{(2S+1)} L_Jq)|_{\hat{t}\leftrightarrow\hat{u}} \tag{A2}$$

- g g $\rightarrow$ $^{(2S+1)}L_J$ g

$$
\begin{aligned}
\frac{d\sigma}{d\hat{t}}(^3S_1) =& \frac{5\pi {\alpha_s}^3 (R_0)^2}{9M\hat{s}^2} \cdot \frac{M^2}{(\hat{s}-M^2)^2(\hat{t}-M^2)^2(\hat{u}-M^2)^2} \\
& \cdot \{[\hat{s}^2(\hat{s}-M^2)^2] + [\hat{s} \rightarrow \hat{t}] + [\hat{s} \rightarrow \hat{u}]\} \\
\frac{d\sigma}{d\hat{t}}(^1S_0) =& \frac{\pi {\alpha_s}^3 (R_0)^2}{2M\hat{s}^2} \frac{1}{\hat{s}\hat{t}\hat{u}(\hat{s}-M^2)^2(\hat{t}-M^2)^2(\hat{u}-M^2)^2} \\
& \cdot \{[\hat{s}^4(\hat{s}-M^2)^2((\hat{s}-M^2)^2 + 2M^4) \\
& - \frac{4}{3}\hat{s}\hat{t}\hat{u}(\hat{s}^2+\hat{t}^2+\hat{u}^2)(\hat{s}-M^2)(\hat{t}-M^2)(\hat{u}-M^2) \\
& + \frac{16}{3}M^2\hat{s}\hat{t}\hat{u}(\hat{s}^2\hat{t}^2+\hat{s}^2\hat{u}^2+\hat{t}^2\hat{u}^2) \\
& + \frac{28}{3}M^4\hat{s}^2\hat{t}^2\hat{u}^2] + [\hat{s} \leftrightarrow \hat{t}] + [\hat{s} \leftrightarrow \hat{u}]\}
\end{aligned}
\tag{A3}
$$

We define two new variables as a combination of $\hat{s}$, $\hat{t}$ and $\hat{u}$ which can be used to define the g g $\rightarrow$ $^{(2S+1)}L_J$ g cross sections.

$$
\begin{aligned}
P &= \hat{s}\hat{t} + \hat{t}\hat{u} + \hat{u}\hat{s} \\
Q &= \hat{s}\hat{t}\hat{u}
\end{aligned}
\tag{A4}
$$

$$
\begin{aligned}
\frac{d\sigma}{d\hat{t}}({}^1S_0) &= \frac{\pi {\alpha_s}^3 (R_0)^2}{M\hat{s}^2}\frac{P^2(M^8-2M^4P+P^2+2M^2Q)}{Q(Q-M^2P)^2} \\
\frac{d\sigma}{d\hat{t}}({}^3S_1) &= \frac{10\pi {\alpha_s}^3 (R_0)^2}{9\hat{s}^2}\frac{M(P^2-M^2Q)}{(Q-M^2P)^2} \\
\frac{d\sigma}{d\hat{t}}({}^1P_1) &= \frac{40\pi {\alpha_s}^3 (R_1')^2}{3M\hat{s}^2}\frac{[-M^{10}P+M^6P^2+Q(5M^8-7M^4P+2P^2)+4M^2Q^2]}{(Q-M^2P)^3} \\
\frac{d\sigma}{d\hat{t}}({}^3P_0) &= \frac{4\pi {\alpha_s}^3 (R_1')^2}{M^3\hat{s}^2}\frac{1}{Q(Q-M^2P)^4}[9M^4P^4(M^8-2M^4P+P^2) \\
&\quad -6M^2P^3Q(2M^8-5M^4P+P^2) \\
&\quad -P^2Q^2(M^8+2M^4P-P^2) \\
&\quad +2M^2PQ^3(M^4-P)+6M^4Q^4] \\
\frac{d\sigma}{d\hat{t}}({}^3P_1) &= \frac{12\pi {\alpha_s}^3 (R_1')^2}{M^3\hat{s}^2}\frac{P^2\{M^2P^2(M^4-4P)-2Q(M^8-5M^4P-P^2)-15M^2Q^2\}}{(Q-M^2P)^4} \\
\frac{d\sigma}{d\hat{t}}({}^3P_2) &= \frac{4\pi {\alpha_s}^3 (R_1')^2}{M^3\hat{s}^2}\frac{1}{Q(Q-M^2P)^4} \\
&\quad \{12M^4P^4(M^8-2M^4P+P^2)-3M^2P^3Q(8M^8-M^4P+4P^2) \\
&\quad -2P^2Q^2(7M^8-43M^4P-P^2)+M^2PQ^3(16M^4-61P) \\
&\quad +12M^4Q^4\}
\end{aligned}
\tag{A5}
$$

b. **Color Octet PQCD cross sections**

We list below short distance squared amplitudes for $2 \to 2$ scattering processes which mediate color-octet quarkonia production. These expressions are averaged over initial spins and colors of the two incident partons. The helicity levels of outgoing $J = 1$ and $J = 2$ pairs are labeled by the subscript h.

- $\mathrm{q}\ \bar{\mathrm{q}} \to Q\bar{Q}[^{(2\mathrm{S}+1)}\mathrm{L}_{\mathrm{J}}^{(8)}]\ \mathrm{g}$

$$
\begin{aligned}
\bar{\sum} |\mathcal{A}(q\bar{q} \to Q\overline{Q}[^1S_0^{(8)}]g)|^2 &= \frac{5(4\pi\alpha_s)^3}{27M}\frac{\hat{t}^2+\hat{u}^2}{\hat{s}(\hat{s}-M^2)^2} \\
\bar{\sum_{h=0}} |\mathcal{A}(q\bar{q} \to Q\overline{Q}[^3S_1^{(8)}]g)|^2 &= \frac{8(4\pi\alpha_s)^3}{81M^3}\frac{M^2\hat{\mathrm{s}}}{(\hat{\mathrm{s}}-M^2)^4}\left[4(\hat{\mathrm{t}}^2+\hat{\mathrm{u}}^2)-\hat{\mathrm{t}}\hat{\mathrm{u}}\right] \\
\bar{\sum_{|h|=1}} |\mathcal{A}(q\bar{q} \to Q\overline{Q}[^3S_1^{(8)}]g)|^2 &= \frac{2(4\pi\alpha_s)^3}{81M^3}\frac{\hat{\mathrm{s}}^2+M^4}{(\hat{\mathrm{s}}-M^2)^4}\frac{\hat{\mathrm{t}}^2+\hat{\mathrm{u}}^2}{\hat{\mathrm{t}}\hat{\mathrm{u}}}\left[4(\hat{\mathrm{t}}^2+\hat{\mathrm{u}}^2)-\hat{\mathrm{t}}\hat{\mathrm{u}}\right] \\
\bar{\sum} |\mathcal{A}(q\bar{q} \to Q\overline{Q}[^3P_0^{(8)}]g)|^2 &= \frac{20(4\pi\alpha_s)^3}{81M^3}\frac{(\hat{\mathrm{s}}-3M^2)^2(\hat{\mathrm{t}}^2+\hat{\mathrm{u}}^2)}{\hat{\mathrm{s}}(\hat{\mathrm{s}}-M^2)^4} \\
\bar{\sum_{h=0}} |\mathcal{A}(q\bar{q} \to Q\overline{Q}[^3P_1^{(8)}]g)|^2 &= \frac{40(4\pi\alpha_s)^3}{81M^3}\frac{\hat{\mathrm{s}}(\hat{\mathrm{t}}^2+\hat{\mathrm{u}}^2)}{(\hat{\mathrm{s}}-M^2)^4} \\
\bar{\sum_{|h|=1}} |\mathcal{A}(q\bar{q} \to Q\overline{Q}[^3P_1^{(8)}]g)|^2 &= \frac{160(4\pi\alpha_s)^3}{81M^3}\frac{M^2\hat{\mathrm{t}}\hat{\mathrm{u}}}{(\hat{\mathrm{s}}-M^2)^4} \\
\bar{\sum_{h=0}} |\mathcal{A}(q\bar{q} \to Q\overline{Q}[^3P_2^{(8)}]g)|^2 &= \frac{8(4\pi\alpha_s)^3}{81M^3}\frac{\hat{\mathrm{s}}(\hat{\mathrm{t}}^2+\hat{\mathrm{u}}^2)}{(\hat{\mathrm{s}}-M^2)^4} \\
\bar{\sum_{|h|=1}} |\mathcal{A}(q\bar{q} \to Q\overline{Q}[^3P_2^{(8)}]g)|^2 &= \frac{32(4\pi\alpha_s)^3}{27M^3}\frac{M^2\hat{\mathrm{t}}\hat{\mathrm{u}}}{(\hat{\mathrm{s}}-M^2)^4} \\
\bar{\sum_{|h|=2}} |\mathcal{A}(q\bar{q} \to Q\overline{Q}[^3P_2^{(8)}]g)|^2 &= \frac{16(4\pi\alpha_s)^3}{27M^3}\frac{M^4(\hat{\mathrm{t}}^2+\hat{\mathrm{u}}^2)}{\hat{\mathrm{s}}(\hat{\mathrm{s}}-M^2)^4}
\end{aligned}
\tag{A6}
$$

- g q $\to Q\bar{Q}[^{(2S+1)}\mathrm{L}_\mathrm{J}^{(8)}]$ q

$$
\begin{aligned}
\bar{\sum}|\mathcal{A}(gq\to Q\overline{Q}[^1S_0^{(8)}]q)|^2 &= -\frac{5(4\pi\alpha_s)^3}{72M}\frac{\hat{\mathrm{s}}^2+\hat{\mathrm{u}}^2}{\hat{\mathrm{t}}(\hat{\mathrm{t}}-M^2)^2}\\
\bar{\sum_{h=0}}|\mathcal{A}(gq\to Q\overline{Q}[^3S_1^{(8)}]q)|^2 &= -\frac{(4\pi\alpha_s)^3}{54M^3}\frac{M^2\hat{\mathrm{t}}\big[4(\hat{\mathrm{s}}^2+\hat{\mathrm{u}}^2)-\hat{\mathrm{s}}\hat{\mathrm{u}}\big]}{\big[(\hat{\mathrm{s}}-M^2)(\hat{\mathrm{t}}-M^2)\big]^2}\\
\bar{\sum_{|h|=1}}|\mathcal{A}(gq\to Q\overline{Q}[^3S_1^{(8)}]q)|^2 &= -\frac{(4\pi\alpha_s)^3}{108M^3}\\
&\quad\times\frac{(\hat{\mathrm{s}}^2+\hat{\mathrm{u}}^2+2M^2\hat{\mathrm{t}})(\hat{\mathrm{s}}-M^2)^2-2M^2\hat{\mathrm{s}}\hat{\mathrm{t}}\hat{\mathrm{u}}}{\hat{\mathrm{s}}\hat{\mathrm{u}}\big[(\hat{\mathrm{s}}-M^2)(\hat{\mathrm{t}}-M^2)\big]^2}\\
&\quad\times\big[4(\hat{\mathrm{s}}^2+\hat{\mathrm{u}}^2)-\hat{\mathrm{s}}\hat{\mathrm{u}}\big]\\
\bar{\sum}|\mathcal{A}(gq\to Q\overline{Q}[^3P_0^{(8)}]q)|^2 &= -\frac{5(4\pi\alpha_s)^3}{54M^3}\frac{(\hat{\mathrm{t}}-3M^2)^2(\hat{\mathrm{s}}^2+\hat{\mathrm{u}}^2)}{\hat{\mathrm{t}}(\hat{\mathrm{t}}-M^2)^4}\\
\bar{\sum_{h=0}}|\mathcal{A}(gq\to Q\overline{Q}[^3P_1^{(8)}]q)|^2 &= -\frac{5(4\pi\alpha_s)^3}{27M^3}\frac{\hat{\mathrm{t}}\big[\hat{\mathrm{s}}^2(\hat{\mathrm{s}}-M^2)^2+\hat{\mathrm{u}}^2(\hat{\mathrm{s}}+M^2)^2\big]}{(\hat{\mathrm{t}}-M^2)^4(\hat{\mathrm{s}}-M^2)^2}\\
\bar{\sum_{|h|=1}}|\mathcal{A}(gq\to Q\overline{Q}[^3P_1^{(8)}]q)|^2 &= -\frac{20(4\pi\alpha_s)^3}{27M^3}\frac{M^2\hat{\mathrm{s}}\hat{\mathrm{u}}(\hat{\mathrm{t}}^2+\hat{\mathrm{t}}\hat{\mathrm{u}}+\hat{\mathrm{u}}^2)}{(\hat{\mathrm{t}}-M^2)^4(\hat{\mathrm{s}}-M^2)^2}\\
\bar{\sum_{h=0}}|\mathcal{A}(gq\to Q\overline{Q}[^3P_2^{(8)}]q)|^2 &= -\frac{(4\pi\alpha_s)^3}{27M^3}\frac{\hat{\mathrm{t}}}{(\hat{\mathrm{t}}-M^2)^4}\\
&\quad\times\big[\hat{\mathrm{s}}^2+\hat{\mathrm{u}}^2+12M^2\hat{\mathrm{s}}\hat{\mathrm{u}}^2\frac{\hat{\mathrm{s}}^2+M^2\hat{\mathrm{s}}+M^4}{(\hat{\mathrm{s}}-M^2)^4}\big]\\
\bar{\sum_{|h|=1}}|\mathcal{A}(gq\to Q\overline{Q}[^3P_2^{(8)}]q)|^2 &= -\frac{4(4\pi\alpha_s)^3}{9M^3}\frac{M^2\hat{\mathrm{s}}\hat{\mathrm{u}}}{(\hat{\mathrm{t}}-M^2)^4}\\
&\quad\times\frac{(\hat{\mathrm{s}}-M^2)^2(\hat{\mathrm{s}}^2+M^4)-(\hat{\mathrm{s}}+M^2)^2\hat{\mathrm{t}}\hat{\mathrm{u}}}{(\hat{\mathrm{s}}-M^2)^4}\\
\bar{\sum_{|h|=2}}|\mathcal{A}(gq\to Q\overline{Q}[^3P_2^{(8)}]q)|^2 &= -\frac{2(4\pi\alpha_s)^3}{9M^3}\frac{M^4}{\hat{\mathrm{t}}(\hat{\mathrm{t}}-M^2)^4}\\
&\quad\times\big[\hat{\mathrm{s}}^2+\hat{\mathrm{u}}^2+2\hat{\mathrm{s}}^2\hat{\mathrm{t}}\hat{\mathrm{u}}\frac{(\hat{\mathrm{s}}-M^2)(2\hat{\mathrm{t}}+\hat{\mathrm{u}})-\hat{\mathrm{u}}^2}{(\hat{\mathrm{s}}-M^2)^4}\big]
\end{aligned}
\tag{A7}
$$

- g g $\to Q\bar{Q}[^{(2S+1)}\mathrm{L}_\mathrm{J}^{(8)}]$ g (The $gg\to Q\overline{Q}[^3P_J^{(8)}]$ g squared amplitudes are expressed in

terms of the variables $\hat{\mathrm{s}}$ and $\hat{\mathrm{z}} \equiv \sqrt{\hat{\mathrm{t}}\hat{\mathrm{u}}}$.)

$$
\begin{aligned}
\bar{\sum} |\mathcal{A}(gg \to Q\overline{Q}[^1S_0^{(8)}]g)|^2 &= \frac{5(4\pi\alpha_s)^3}{16M}\big[\hat{\mathrm{s}}^2(\hat{\mathrm{s}}-M^2)^2 + \hat{\mathrm{s}}\hat{\mathrm{t}}\hat{\mathrm{u}}(M^2-2\hat{\mathrm{s}}) + (\hat{\mathrm{t}}\hat{\mathrm{u}})^2\big] \\
&\quad \times \frac{(\hat{\mathrm{s}}^2 - M^2\hat{\mathrm{s}} + M^4)^2 - \hat{\mathrm{t}}\hat{\mathrm{u}}(2\hat{\mathrm{t}}^2 + 3\hat{\mathrm{t}}\hat{\mathrm{u}} + 2\hat{\mathrm{u}}^2)}{\hat{\mathrm{s}}\hat{\mathrm{t}}\hat{\mathrm{u}}\big[(\hat{\mathrm{s}}-M^2)(\hat{\mathrm{t}}-M^2)(\hat{\mathrm{u}}-M^2)\big]^2} \\
\sum_{h=0}^{\bar{}} |\mathcal{A}(gg \to Q\overline{Q}[^3S_1^{(8)}]g)|^2 &= -\frac{(4\pi\alpha_s)^3}{144M^3}\frac{2M^2\hat{\mathrm{s}}}{(\hat{\mathrm{s}}-M^2)^2}(\hat{\mathrm{t}}^2+\hat{\mathrm{u}}^2)\hat{\mathrm{t}}\hat{\mathrm{u}} \\
&\quad \times \frac{27(\hat{\mathrm{s}}\hat{\mathrm{t}} + \hat{\mathrm{t}}\hat{\mathrm{u}} + \hat{\mathrm{u}}\hat{\mathrm{s}}) - 19M^4}{\big[(\hat{\mathrm{s}}-M^2)(\hat{\mathrm{t}}-M^2)(\hat{\mathrm{u}}-M^2)\big]^2} \\
\sum_{|h|=1}^{\bar{}} |\mathcal{A}(gg \to Q\overline{Q}[^3S_1^{(8)}]g)|^2 &= -\frac{(4\pi\alpha_s)^3}{144M^3}\frac{\hat{\mathrm{s}}^2}{(\hat{\mathrm{s}}-M^2)^2} \\
&\quad \times \big[(\hat{\mathrm{s}}-M^2)^4 + \hat{\mathrm{t}}^4 + \hat{\mathrm{u}}^4 + 2M^4\big(\frac{\hat{\mathrm{t}}\hat{\mathrm{u}}}{\hat{\mathrm{s}}}\big)^2\big] \\
&\quad \times \frac{27(\hat{\mathrm{s}}\hat{\mathrm{t}} + \hat{\mathrm{t}}\hat{\mathrm{u}} + \hat{\mathrm{u}}\hat{\mathrm{s}}) - 19M^4}{\big[(\hat{\mathrm{s}}-M^2)(\hat{\mathrm{t}}-M^2)(\hat{\mathrm{u}}-M^2)\big]^2} \\
\bar{\sum} |\mathcal{A}(gg \to Q\overline{Q}[^3P_0^{(8)}]g)|^2 &= \frac{5(4\pi\alpha_s)^3}{12M^3}\frac{1}{\big[\hat{\mathrm{s}}\hat{\mathrm{z}}^2(\hat{\mathrm{s}}-M^2)^4(\hat{\mathrm{s}}M^2+\hat{\mathrm{z}}^2)^4\big]} \\
&\quad \times \Big\{\hat{\mathrm{s}}^2\hat{\mathrm{z}}^4(\hat{\mathrm{s}}^2-\hat{\mathrm{z}}^2)^4 + M^2\hat{\mathrm{s}}\hat{\mathrm{z}}^2(\hat{\mathrm{s}}^2-\hat{\mathrm{z}}^2)^2(3\hat{\mathrm{s}}^2-2\hat{\mathrm{z}}^2)(2\hat{\mathrm{s}}^4-6\hat{\mathrm{s}}^2\hat{\mathrm{z}}^2+3\hat{\mathrm{z}}^4) \\
&\quad + M^4\big[9\hat{\mathrm{s}}^{12} - 84\hat{\mathrm{s}}^{10}\hat{\mathrm{z}}^2 + 265\hat{\mathrm{s}}^8\hat{\mathrm{z}}^4 - 382\hat{\mathrm{s}}^6\hat{\mathrm{z}}^6 + 276\hat{\mathrm{s}}^4\hat{\mathrm{z}}^8 - 88\hat{\mathrm{s}}^2\hat{\mathrm{z}}^{10} + 9\hat{\mathrm{z}}^{12}\big] \\
&\quad - M^6\hat{\mathrm{s}}\big[54\hat{\mathrm{s}}^{10} - 357\hat{\mathrm{s}}^8\hat{\mathrm{z}}^2 + 844\hat{\mathrm{s}}^6\hat{\mathrm{z}}^4 - 898\hat{\mathrm{s}}^4\hat{\mathrm{z}}^6 + 439\hat{\mathrm{s}}^2\hat{\mathrm{z}}^8 - 81\hat{\mathrm{z}}^{10}\big] \\
&\quad + M^8\big[153\hat{\mathrm{s}}^{10} - 798\hat{\mathrm{s}}^8\hat{\mathrm{z}}^2 + 1415\hat{\mathrm{s}}^6\hat{\mathrm{z}}^4 - 1041\hat{\mathrm{s}}^4\hat{\mathrm{z}}^6 + 301\hat{\mathrm{s}}^2\hat{\mathrm{z}}^8 - 18\hat{\mathrm{z}}^{10}\big] \\
&\quad - M^{10}\hat{\mathrm{s}}\big[270\hat{\mathrm{s}}^8 - 1089\hat{\mathrm{s}}^6\hat{\mathrm{z}}^2 + 1365\hat{\mathrm{s}}^4\hat{\mathrm{z}}^4 - 616\hat{\mathrm{s}}^2\hat{\mathrm{z}}^6 + 87\hat{\mathrm{z}}^8\big] \\
&\quad + M^{12}\big[324\hat{\mathrm{s}}^8 - 951\hat{\mathrm{s}}^6\hat{\mathrm{z}}^2 + 769\hat{\mathrm{s}}^4\hat{\mathrm{z}}^4 - 189\hat{\mathrm{s}}^2\hat{\mathrm{z}}^6 + 9\hat{\mathrm{z}}^8\big] \\
&\quad - 9M^{14}\hat{\mathrm{s}}\big[(6\hat{\mathrm{s}}^2-\hat{\mathrm{z}}^2)(5\hat{\mathrm{s}}^4 - 9\hat{\mathrm{s}}^2\hat{\mathrm{z}}^2 + 3\hat{\mathrm{z}}^4)\big] \\
&\quad + 3M^{16}\hat{\mathrm{s}}^2\big[51\hat{\mathrm{s}}^4 - 59\hat{\mathrm{s}}^2\hat{\mathrm{z}}^2 + 12\hat{\mathrm{z}}^4\big] \\
&\quad - 27M^{18}\hat{\mathrm{s}}^3\big[2\hat{\mathrm{s}}^2 - \hat{\mathrm{z}}^2\big] \\
&\quad + 9M^{20}\hat{\mathrm{s}}^4\Big\}
\end{aligned}
\tag{A8}
$$

$$
\begin{aligned}
\sum_{h=0}^{-}|\mathcal{A}(gg\to Q\overline{Q}[^3P_1^{(8)}]g)|^2 &= \frac{5(4\pi\alpha_s)^3}{6M^3}\frac{1}{\left[(\hat{\mathrm{s}}-M^2)^4(\hat{\mathrm{s}}M^2+\hat{\mathrm{z}}^2)^4\right]}\\
&\times \hat{\mathrm{s}}\hat{\mathrm{z}}^2\left[(\hat{\mathrm{s}}^2-\hat{\mathrm{z}}^2)^2-2M^2\hat{\mathrm{s}}\hat{\mathrm{z}}^2-M^4(\hat{\mathrm{s}}^2+2\hat{\mathrm{z}}^2)+M^8\right]\\
&\times \left[(\hat{\mathrm{s}}^2-\hat{\mathrm{z}}^2)^2-M^2\hat{\mathrm{s}}(2\hat{\mathrm{s}}^2-\hat{\mathrm{z}}^2)+M^4\hat{\mathrm{s}}^2\right]\\
\sum_{|h|=1}^{-}|\mathcal{A}(gg\to Q\overline{Q}[^3P_1^{(8)}]g)|^2 &= \frac{5(4\pi\alpha_s)^3}{6M^3}\frac{1}{\left[(\hat{\mathrm{s}}-M^2)^4(\hat{\mathrm{s}}M^2+\hat{\mathrm{z}}^2)^4\right]}\\
&\times M^2\Big\{2(\hat{\mathrm{s}}^2-\hat{\mathrm{z}}^2)^2(\hat{\mathrm{s}}^6-4\hat{\mathrm{s}}^4\hat{\mathrm{z}}^2+\hat{\mathrm{s}}^2\hat{\mathrm{z}}^4-\hat{\mathrm{z}}^6)\\
&- M^2\hat{\mathrm{s}}(2\hat{\mathrm{s}}^2-\hat{\mathrm{z}}^2)(5\hat{\mathrm{s}}^6-17\hat{\mathrm{s}}^4\hat{\mathrm{z}}^2+9\hat{\mathrm{s}}^2\hat{\mathrm{z}}^4-\hat{\mathrm{z}}^6)\\
&+ M^4(21\hat{\mathrm{s}}^8-49\hat{\mathrm{s}}^6\hat{\mathrm{z}}^2+21\hat{\mathrm{s}}^4\hat{\mathrm{z}}^4-4\hat{\mathrm{s}}^2\hat{\mathrm{z}}^6+\hat{\mathrm{z}}^8)\\
&- M^6\hat{\mathrm{s}}(24\hat{\mathrm{s}}^6-30\hat{\mathrm{s}}^4\hat{\mathrm{z}}^2+6\hat{\mathrm{s}}^2\hat{\mathrm{z}}^4-\hat{\mathrm{z}}^6)\\
&+ M^8\hat{\mathrm{s}}^2(16\hat{\mathrm{s}}^4-9\hat{\mathrm{s}}^2\hat{\mathrm{z}}^2+2\hat{\mathrm{z}}^4)\\
&- M^{10}\hat{\mathrm{s}}^3(6\hat{\mathrm{s}}^2-\hat{\mathrm{z}}^2)\\
&+ M^{12}\hat{\mathrm{s}}^4\Big\}
\end{aligned}
\tag{A9}
$$

$$
\begin{aligned}
\sum_{h=0}^{-}|\mathcal{A}(gg\to Q\overline{Q}[^3P_2^{(8)}]g)|^2 &= \frac{(4\pi\alpha_s)^3}{6M^3}\frac{\hat{\mathrm{s}}\hat{\mathrm{z}}^2}{\left[(\hat{\mathrm{s}}-M^2)^6(\hat{\mathrm{s}}M^2+\hat{\mathrm{z}}^2)^4\right]}\\
&\Big\{\hat{\mathrm{s}}^2(\hat{\mathrm{s}}^2-\hat{\mathrm{z}}^2)^4-M^2\hat{\mathrm{s}}\hat{\mathrm{z}}^2(\hat{\mathrm{s}}^2-\hat{\mathrm{z}}^2)^2(11\hat{\mathrm{s}}^2+2\hat{\mathrm{z}}^2)\\
&+ M^4\left[\hat{\mathrm{s}}^8-12\hat{\mathrm{s}}^6\hat{\mathrm{z}}^2+41\hat{\mathrm{s}}^4\hat{\mathrm{z}}^4-20\hat{\mathrm{s}}^2\hat{\mathrm{z}}^6+\hat{\mathrm{z}}^8\right]\\
&- M^6\hat{\mathrm{s}}\left[4\hat{\mathrm{s}}^6-26\hat{\mathrm{s}}^4\hat{\mathrm{z}}^2-\hat{\mathrm{s}}^2\hat{\mathrm{z}}^4-5\hat{\mathrm{z}}^6\right]\\
&+ M^8\left[29\hat{\mathrm{s}}^6-114\hat{\mathrm{s}}^4\hat{\mathrm{z}}^2+108\hat{\mathrm{s}}^2\hat{\mathrm{z}}^4-10\hat{\mathrm{z}}^6\right]\\
&- M^{10}\hat{\mathrm{s}}\left[65\hat{\mathrm{s}}^4-104\hat{\mathrm{s}}^2\hat{\mathrm{z}}^2-33\hat{\mathrm{z}}^4\right]\\
&+ M^{12}\left[54\hat{\mathrm{s}}^4-20\hat{\mathrm{s}}^2\hat{\mathrm{z}}^2+7\hat{\mathrm{z}}^4\right]\\
&- M^{14}\hat{\mathrm{s}}\left[23\hat{\mathrm{s}}^2+5\hat{\mathrm{z}}^2\right]\\
&+ 7M^{16}\hat{\mathrm{s}}^2\Big\}
\end{aligned}
$$

$$
\begin{aligned}
\bar{\sum_{|h|=1}} |\mathcal{A}(gg \to Q\overline{Q}[^3P_2^{(8)}]g)|^2 &= \frac{(4\pi\alpha_s)^3}{2M^3}\frac{M^2}{\left[(\hat{\mathrm{s}}-M^2)^6(\hat{\mathrm{s}}M^2+\hat{\mathrm{z}}^2)^4\right]} \\
&\times \Big\{2\hat{\mathrm{s}}^2(\hat{\mathrm{s}}^2-\hat{\mathrm{z}}^2)^2(\hat{\mathrm{s}}^6-4\hat{\mathrm{s}}^4\hat{\mathrm{z}}^2+\hat{\mathrm{s}}^2\hat{\mathrm{z}}^4-\hat{\mathrm{z}}^6) \\
&- M^2\hat{\mathrm{s}}\big[10\hat{\mathrm{s}}^{10}-37\hat{\mathrm{s}}^8\hat{\mathrm{z}}^2+19\hat{\mathrm{s}}^6\hat{\mathrm{z}}^4+11\hat{\mathrm{s}}^4\hat{\mathrm{z}}^6-\hat{\mathrm{s}}^2\hat{\mathrm{z}}^8-4\hat{\mathrm{z}}^{10}\big] \\
&+ M^4\big[25\hat{\mathrm{s}}^{10}-61\hat{\mathrm{s}}^8\hat{\mathrm{z}}^2+27\hat{\mathrm{s}}^6\hat{\mathrm{z}}^4-34\hat{\mathrm{s}}^4\hat{\mathrm{z}}^6+23\hat{\mathrm{s}}^2\hat{\mathrm{z}}^8-2\hat{\mathrm{z}}^{10}\big] \\
&- M^6\hat{\mathrm{s}}\big[42\hat{\mathrm{s}}^8-77\hat{\mathrm{s}}^6\hat{\mathrm{z}}^2+41\hat{\mathrm{s}}^4\hat{\mathrm{z}}^4-22\hat{\mathrm{s}}^2\hat{\mathrm{z}}^6+17\hat{\mathrm{z}}^8\big] \\
&+ M^8\big[53\hat{\mathrm{s}}^8-88\hat{\mathrm{s}}^6\hat{\mathrm{z}}^2+69\hat{\mathrm{s}}^4\hat{\mathrm{z}}^4-68\hat{\mathrm{s}}^2\hat{\mathrm{z}}^6+3\hat{\mathrm{z}}^8\big] \\
&- M^{10}\hat{\mathrm{s}}\big[54\hat{\mathrm{s}}^6-85\hat{\mathrm{s}}^4\hat{\mathrm{z}}^2+60\hat{\mathrm{s}}^2\hat{\mathrm{z}}^4-9\hat{\mathrm{z}}^6\big] \\
&+ M^{12}\hat{\mathrm{s}}^2\big[43\hat{\mathrm{s}}^4-47\hat{\mathrm{s}}^2\hat{\mathrm{z}}^2+20\hat{\mathrm{z}}^4\big] \\
&- M^{14}\hat{\mathrm{s}}^3\big[22\hat{\mathrm{s}}^2-9\hat{\mathrm{z}}^2\big] \\
&+ 5M^{16}\hat{\mathrm{s}}^4\Big\} \\
\bar{\sum_{|h|=2}} |\mathcal{A}(gg \to Q\overline{Q}[^3P_2^{(8)}]g)|^2 &= \frac{(4\pi\alpha_s)^3}{2M^3}\frac{M^4}{\left[\hat{\mathrm{s}}\hat{\mathrm{z}}^2(\hat{\mathrm{s}}-M^2)^6(\hat{\mathrm{s}}M^2+\hat{\mathrm{z}}^2)^4\right]} \\
&\times \Big\{2\hat{\mathrm{s}}^2\big[\hat{\mathrm{s}}^{12}-8\hat{\mathrm{s}}^{10}\hat{\mathrm{z}}^2+22\hat{\mathrm{s}}^8\hat{\mathrm{z}}^4-24\hat{\mathrm{s}}^6\hat{\mathrm{z}}^6+10\hat{\mathrm{s}}^4\hat{\mathrm{z}}^8-3\hat{\mathrm{s}}^2\hat{\mathrm{z}}^{10}+\hat{\mathrm{z}}^{12}\big] \\
&- M^2\hat{\mathrm{s}}\big[16\hat{\mathrm{s}}^{12}-102\hat{\mathrm{s}}^{10}\hat{\mathrm{z}}^2+210\hat{\mathrm{s}}^8\hat{\mathrm{z}}^4-153\hat{\mathrm{s}}^6\hat{\mathrm{z}}^6+36\hat{\mathrm{s}}^4\hat{\mathrm{z}}^8-6\hat{\mathrm{s}}^2\hat{\mathrm{z}}^{10}+4\hat{\mathrm{z}}^{12}\big] \\
&+ M^4\big[60\hat{\mathrm{s}}^{12}-306\hat{\mathrm{s}}^{10}\hat{\mathrm{z}}^2+482\hat{\mathrm{s}}^8\hat{\mathrm{z}}^4-271\hat{\mathrm{s}}^6\hat{\mathrm{z}}^6+77\hat{\mathrm{s}}^4\hat{\mathrm{z}}^8-18\hat{\mathrm{s}}^2\hat{\mathrm{z}}^{10}+2\hat{\mathrm{z}}^{12}\big] \\
&- M^6\hat{\mathrm{s}}\big[140\hat{\mathrm{s}}^{10}-573\hat{\mathrm{s}}^8\hat{\mathrm{z}}^2+710\hat{\mathrm{s}}^6\hat{\mathrm{z}}^4-344\hat{\mathrm{s}}^4\hat{\mathrm{z}}^6+91\hat{\mathrm{s}}^2\hat{\mathrm{z}}^8-18\hat{\mathrm{z}}^{10}\big] \\
&+ M^8\big[226\hat{\mathrm{s}}^{10}-741\hat{\mathrm{s}}^8\hat{\mathrm{z}}^2+737\hat{\mathrm{s}}^6\hat{\mathrm{z}}^4-310\hat{\mathrm{s}}^4\hat{\mathrm{z}}^6+77\hat{\mathrm{s}}^2\hat{\mathrm{z}}^8-4\hat{\mathrm{z}}^{10}\big] \\
&- M^{10}\hat{\mathrm{s}}\big[264\hat{\mathrm{s}}^8-686\hat{\mathrm{s}}^6\hat{\mathrm{z}}^2+541\hat{\mathrm{s}}^4\hat{\mathrm{z}}^4-177\hat{\mathrm{s}}^2\hat{\mathrm{z}}^6+25\hat{\mathrm{z}}^8\big] \\
&+ M^{12}\big[226\hat{\mathrm{s}}^8-452\hat{\mathrm{s}}^6\hat{\mathrm{z}}^2+261\hat{\mathrm{s}}^4\hat{\mathrm{z}}^4-55\hat{\mathrm{s}}^2\hat{\mathrm{z}}^6+2\hat{\mathrm{z}}^8\big] \\
&- M^{14}\hat{\mathrm{s}}\big[140\hat{\mathrm{s}}^6-201\hat{\mathrm{s}}^4\hat{\mathrm{z}}^2+71\hat{\mathrm{s}}^2\hat{\mathrm{z}}^4-6\hat{\mathrm{z}}^6\big] \\
&+ M^{16}\hat{\mathrm{s}}^2\big[60\hat{\mathrm{s}}^4-53\hat{\mathrm{s}}^2\hat{\mathrm{z}}^2+8\hat{\mathrm{z}}^4\big] \\
&- 2M^{18}\hat{\mathrm{s}}^3\big[8\hat{\mathrm{s}}^2-3\hat{\mathrm{z}}^2\big] \\
&+ 2M^{20}\hat{\mathrm{s}}^4\Big\}
\end{aligned}
\tag{A10}
$$

[1] J. E. Augustin *et al.* [SLAC-SP-017 Collaboration], "Discovery of a Narrow Resonance in e+ e- Annihilation," Phys. Rev. Lett. **33**, 1406 (1974) [Adv. Exp. Phys. **5**, 141 (1976)].

[2] J. J. Aubert *et al.* [E598 Collaboration], "Experimental Observation of a Heavy Particle J," Phys. Rev. Lett. **33**, 1404 (1974). doi:10.1103/PhysRevLett.33.1404

[3] P. Nason, S. Dawson and R. K. Ellis, "The Total Cross-Section For The Production Of Heavy Quarks In Hadronic Collisions," Nucl. Phys. B **303** (1988) 607;

[4] P. Nason, S. Dawson and R. K. Ellis, "The One Particle Inclusive Differential Cross-Section For Heavy Quark Production In Hadronic Collisions," Nucl. Phys. B **327** (1989) 49 [Erratum-ibid. B **335** (1990) 260].

[5] G. T. Bodwin, E. Braaten, and G. P. Lepage, "Rigorous QCD analysis of inclusive annihilation and production of heavy quarkonium," Phys. Rev. D **51** 1125 (1995), [Erratum-ibid. D **55** 5853 (1997)], arXiv:hep-ph/9407339.

[6] N. Brambilla *et al.*, Heavy quarkonium physics, CERN-2005-005, (CERN, Geneva, 2005), arXiv:hep-ph/0412158.

[7] M. B. Einhorn and S. D. Ellis, "Hadronic Production Of The New Resonances: Probing Gluon Distributions," Phys. Rev. D **12** 2007 (1975).

[8] S. D. Ellis, M. B. Einhorn, and C. Quigg, "Comment On Hadronic Production Of Psions," Phys. Rev. Lett. **36** 1263 (1976)

[9] C. E. Carlson and R. Suaya, "Hadronic Production Of Psi/J Mesons," Phys. Rev. D **14** 3115 (1976).

[10] E. L. Berger and D. L. Jones, "Inelastic Photoproduction of J/psi and Upsilon by Gluons," Phys. Rev. D **23**, 1521 (1981).

[11] G. A. Schuler, "Quarkonium production and decays," [arXiv:hep-ph/9403387].

[12] P. Artoisenet, J. P. Lansberg, and F. Maltoni, "Hadroproduction of J/ψ and υ in association with a heavy-quark pair," Phys. Lett. B **653** 60 (2007), [arXiv:hep-ph/0703129]

[13] J. M. Campbell, F. Maltoni, and F. Tramontano, "QCD corrections to J/psi and Upsilon production at hadron colliders," Phys. Rev. Lett. **98** 252002 (2007), [arXiv:hep-ph/0703113]

[14] P. Artoisenet, J. M. Campbell, J. P. Lansberg, F. Maltoni, and F. Tramontano, "Υ Production at Fermilab Tevatron and LHC Energies," Phys. Rev. Lett. **101** 152001 (2008),

[arXiv:0806.3282 [hep-ph]].

[15] H. Fritzsch, "Producing Heavy Quark Flavors in Hadronic Collisions: A Test of Quantum Chromodynamics," Phys. Lett. B **67**, 217 (1977).

[16] J. F. Amundson, O. J. P. Eboli, E. M. Gregores and F. Halzen, "Colorless states in perturbative QCD: Charmonium and rapidity gaps," Phys. Lett. B **372**, 127 (1996), [hep-ph/9512248].

[17] J. F. Amundson, O. J. P. Eboli, E. M. Gregores and F. Halzen, "Quantitative tests of color evaporation: Charmonium production," Phys. Lett. B **390**, 323 (1997), [hep-ph/9605295].

[18] G. C. Nayak, J. W. Qiu, and G. Sterman, "Fragmentation, factorization and infrared poles in heavy quarkonium production," Phys. Lett. B **613** 45 (2005), [arXiv:hep-ph/0501235].

[19] G. C. Nayak, J. W. Qiu, and G. Sterman, "Fragmentation, NRQCD and NNLO factorization analysis in heavy quarkonium production," Phys. Rev. D **72** 114012 (2005), [arXiv:hep-ph/0509021].

[20] E. Braaten, S. Fleming, and T. C. Yuan, "Production of heavy quarkonium in high-energy colliders," Ann. Rev. Nucl. Part. Sci. **46**, 197 (1996), [arXiv:hep-ph/9602374].

[21] B. Gong and J. X. Wang, "Next-to-leading-order QCD corrections to J/ψ polarization at Tevatron and Large-Hadron-Collider energies," Phys. Rev. Lett. **100**, 232001 (2008), [arXiv:0802.3727 [hep-ph]].

[22] B. Gong, X. Q. Li and J. X. Wang, "QCD corrections to J/ψ production via color octet states at Tevatron and LHC," Phys. Lett. B **673**, 197 (2009), [Phys. Lett. **693**, 612 (2010)], [arXiv:0805.4751 [hep-ph]].

[23] Y. Q. Ma, K. Wang and K. T. Chao, "QCD radiative corrections to χ_{cJ} production at hadron colliders," Phys. Rev. D **83**, 111503 (2011), [arXiv:1002.3987 [hep-ph]].

[24] M. Butenschoen and B. A. Kniehl, "J/psi polarization at Tevatron and LHC: Nonrelativistic-QCD factorization at the crossroads," Phys. Rev. Lett. **108**, 172002 (2012), [arXiv:1201.1872 [hep-ph]].

[25] K. T. Chao, Y. Q. Ma, H. S. Shao, K. Wang and Y. J. Zhang, "J/ψ Polarization at Hadron Colliders in Nonrelativistic QCD," Phys. Rev. Lett. **108**, 242004 (2012), [arXiv:1201.2675 [hep-ph]].

[26] B. Gong, L. P. Wan, J. X. Wang and H. F. Zhang, "Polarization for Prompt J/ψ and ψ(2S) Production at the Tevatron and LHC," Phys. Rev. Lett. **110**, no. 4, 042002 (2013), [arXiv:1205.6682 [hep-ph]].

[27] M. Butenschoen and B. A. Kniehl, "Reconciling J/ψ production at HERA, RHIC, Tevatron, and LHC with NRQCD factorization at next-to-leading order," Phys. Rev. Lett. **106**, 022003 (2011),[arXiv:1009.5662 [hep-ph]].

[28] Y. Q. Ma, K. Wang and K. T. Chao, "A complete NLO calculation of the J/ψ and ψ' production at hadron colliders," Phys. Rev. D **84**, 114001 (2011), [arXiv:1012.1030 [hep-ph]].

[29] S. Chatrchyan *et al.* [CMS Collaboration], "J/ψ and ψ_{2S} production in pp collisions at $\sqrt{s} = 7$ TeV," JHEP **1202**, 011 (2012), [arXiv:1111.1557 [hep-ex]].

[30] V. Khachatryan *et al.* [CMS Collaboration], "Measurement of J/ψ and ψ(2S) Prompt Double-Differential Cross Sections in pp Collisions at $\sqrt{s}$=7TeV," Phys. Rev. Lett. **114**, no. 19, 191802 (2015), [arXiv:1502.04155 [hep-ex]].

[31] G. Aad *et al.* [ATLAS Collaboration], "Measurement of the differential cross-sections of prompt and non-prompt production of J/ψ and ψ(2S) in pp collisions at $\sqrt{s} = 7$ and 8 TeV with the ATLAS detector," arXiv:1512.03657 [hep-ex].

[32] D. Acosta *et al.* [CDF Collaboration], "Measurement of the J/ψ meson and $b-$hadron production cross sections in $p\bar{p}$ collisions at $\sqrt{s} = 1960$ GeV," Phys. Rev. D **71**, 032001 (2005).

[33] F. Abe *et al.* [CDF Collaboration], "Production of J/ψ mesons from χ_c meson decays in $p\bar{p}$ collisions at $\sqrt{s} = 1.8$ TeV," Phys. Rev. Lett. **79**, 578 (1997).

[34] R. Baier and R. Ruckl, "Hadronic Collisions: A Quarkonium Factory," Z. Phys. C **19**, 251 (1983).

[35] B. Humpert, "Narrow Heavy Resonance Production By Gluons," Phys. Lett. B **184**, 105 (1987).

[36] R. Gastmans, W. Troost and T. T. Wu, "Production of Heavy Quarkonia From Gluons," Nucl. Phys. B **291**, 731 (1987).

[37] P. L. Cho and A. K. Leibovich, "Color octet quarkonia production," Phys. Rev. D **53**, 150 (1996), [hep-ph/9505329].

[38] P. L. Cho and A. K. Leibovich, "Color octet quarkonia production. 2.," Phys. Rev. D **53**, 6203 (1996), [hep-ph/9511315].

[39] E. Braaten, S. Fleming and A. K. Leibovich, "NRQCD analysis of bottomonium production at the Tevatron," Phys. Rev. D **63**, 094006 (2001), [hep-ph/0008091].

[40] H. L. Lai, M. Guzzi, J. Huston, Z. Li, P. M. Nadolsky, J. Pumplin and C.-P. Yuan, "New parton distributions for collider physics," Phys. Rev. D **82**, 074024 (2010), [arXiv:1007.2241

[hep-ph]].

[41] E. J. Eichten and C. Quigg, "Mesons with beauty and charm: Spectroscopy," Phys. Rev. D **49**, 5845 (1994) [hep-ph/9402210].

[42] K. Nakamura *et al.* [Particle Data Group Collaboration], "Review of particle physics," J. Phys. G **37**, 075021 (2010).